Enhancing Molecular n-Type Doping of Donor-Acceptor Copolymers by Tailoring Side Chains

Liu, Jian; Qiu, Li; Alessandri, Riccardo; Qiu, Xinkai; Portale, Giuseppe; Dong, JingJin; Talsma, Wytse; Ye, Gang; Sengrian, Aprizal Akbar; Souza, Paulo C T

Published in:
Advanced materials

DOI:
10.1002/adma.201704630

ADVANCED MATERIALS

www.advmat.de

Enhancing Molecular n-Type Doping of Donor–Acceptor Copolymers by Tailoring Side Chains

Jian Liu, Li Qiu, Riccardo Alessandri, Xinkai Qiu, Giuseppe Portale, JingJin Dong, Wytse Talsma, Gang Ye, Aprizal Akbar Sengrian, Paulo C. T. Souza, Maria Antonietta Loi, Ryan C. Chiechi, Siewert J. Marrink, Jan C. Hummelen,* and L. Jan Anton Koster**

In this contribution, for the first time, the molecular n-doping of a donor–acceptor (D–A) copolymer achieving 200-fold enhancement of electrical conductivity by rationally tailoring the side chains without changing its D–A backbone is successfully improved. Instead of the traditional alkyl side chains for poly{[*N*,*N*′-bis(2-octyldodecyl)-naphthalene-1,4,5,8-bis(dicarboximide)-2,6-diyl](NDI)-alt-5,5′-(2,2′-bithiophene)} (N2200), polar triethylene glycol type side chains is utilized and a high electrical conductivity of 0.17 S cm^{-1} after doping with (4-(1,3-dimethyl-2,3-dihydro-1H-benzoimidazol-2-yl)phenyl) dimethylamine is achieved, which is the highest reported value for n-type D–A copolymers. Coarse-grained molecular dynamics simulations indicate that the polar side chains can significantly reduce the clustering of dopant molecules and favor the dispersion of the dopant in the host matrix as compared to the traditional alkyl side chains. Accordingly, intimate contact between the host and dopant molecules in the NDI-based copolymer with polar side chains facilitates molecular doping with increased doping efficiency and electrical conductivity. For the first time, a heterogeneous thermoelectric transport model for such a material is proposed, that is the percolation of charge carriers from conducting ordered regions through poorly conductive disordered regions, which provides pointers for further increase in the themoelectric properties of n-type D–A copolymers.

Molecular doping of organic semiconductors represents a key strategy for advancing organic electronic devices, which include organic field-effect transistors, optoelectric devices, and organic thermoelectrics.[1–17] For example, molecular doping is utilized to modulate the carrier density in organic semiconductors to achieve high power factors ($S^2\sigma$, where S and σ are Seebeck coefficient and electrical conductivity, respectively) in the organic thermoelectrics community.[7,12,18–20] The simple implementation of molecular doping by low-temperature solution coprocessing with a host/dopant mixture is one of its intrinsic advantages over other doping strategies, such as electrochemical doping. A key parameter for the evaluation of the molecular doping process is the doping level or relative carrier density. Molecular doping is considered to be governed by many factors, such as the energetics of host molecules, strength of the dopant, miscibility of the host/dopant system, and spatial arrangement between the host and dopant molecules.[21–23] Numerous strategies, such as controlling the host/dopant mixture solution temperature,[24] tuning the strength of the dopants,[25] controlling the morphology of doped films, and synthetically modifying the host,[18,26–28] have been used to enhance molecular doping. Although substantial progress has been made, most of these works were conducted in p-doped conjugated polymers, while doping of their counterparts, n-type conjugated polymers are still not well developed.

Looking back at the history of organic electronics, donor–acceptor (D–A) copolymers play a key role in advancing device performance.[29–33] The most important feature of D–A copolymers is the ability to finely tune their electronic properties via careful selection of the two moieties. However, the intrinsically complex molecular structure brings more challenges to the molecular doping of these systems. The most famous and widely used n-type D–A copolymer is poly{[*N*,*N*′-bis(2-octyldodecyl)-naphthalene-1,4,5,8-bis(dicarboximide)-2,6-diyl](NDI)-alt-5,5′-(2,2′-bithiophene)}(BT) P(NDI2ODT2), called also N2200.[32] Currently, the highest electrical conductivity recorded in doped n-type D–A copolymers is only 1×10^{-3}–5×10^{-3} S cm^{-1}, which was obtained from N2200 doped with molecular dopants, such as (4-(1,3-dimethyl-2,3-dihydro-1H-benzoimidazol-2-yl) phenyl)dimethylamine (n-DMBI).[34–36] However, conjugated polymers without D–A character were recently reported to be efficiently n-doped with the same dopants and to give electrical

Dr. J. Liu, Dr. L. Qiu, R. Alessandri, X. Qiu, Dr. G. Portale, J. Dong, W. Talsma, G. Ye, A. A. Sengrian, Prof. M. A. Loi, Prof. R. C. Chiechi, Prof. S. J. Marrink, Prof. J. C. Hummelen, Prof. L. J. A. Koster
Zernike Institute for Advanced Materials
University of Groningen
Nijenborgh 4, Groningen NL-9747 AG, The Netherlands
E-mail: jian.liu@rug.nl; j.c.hummelen@rug.nl; l.j.a.koster@rug.nl
Dr. L. Qiu, X. Qiu, G. Ye, Prof. R. C. Chiechi, Prof. J. C. Hummelen
Stratingh Institute for Chemistry
University of Groningen
Nijenborgh 4, Groningen NL-9747 AG, The Netherlands
R. Alessandri, Dr. P. C. T. Souza, Prof. S. J. Marrink
Groningen Biomolecular Sciences and Biotechnology Institute
University of Groningen
Nijenborgh 7, Groningen NL-9747 AG, The Netherlands

DOI: 10.1002/adma.201704630

conductivities of 0.18–14 S cm^{-1}.[22,37,38] It is well known that the D–A copolymer has highest occupied molecular orbital and lowest unoccupied molecular orbital (LUMO) spatially distributed on the donor and acceptor moieties, respectively.[39] Previous works suggested that the n-doping of D–A copolymers causes relatively localized charges/polarons on the acceptor moiety in comparison to p-doping.[40,41] Very recently, Wang et al. noted that polarons of doped D–A copolymers were more localized on a single chain than those of doped homopolymers due to an unfavorable distortion of the D–A backbone, which could be a reason for the weak n-doping behavior of D–A copolymers.[38] Bao and co-workers improved the electrical conductivities of n-doped D–A copolymers by minimizing their D–A character via backbone modification.[35] Although different explanations have been proposed, the underlying reason for the weak n-doping of D–A copolymers remains vague, and strategies for enhancing molecular doping in these systems are less explored.

In this contribution, we successfully improved the molecular n-doping of an NDI-based copolymer for the first time with a 200-fold enhancement of its electrical conductivity by rationally tailoring the side chains without changing its D–A backbone. Instead of using traditional alkyl side chains on the acceptor moiety of N2200, we utilized polar triethylene glycol-based side chains and achieved a high electrical conductivity of 0.17 S cm^{-1} after doping with n-DMBI, which is the highest reported value for n-type D–A copolymers. UV–vis absorption spectra, work function, direct measurement of charge carrier density, and Seebeck coefficient measurements confirmed the increased doping level as the primary cause for the improved electrical conductivity. Moreover, coarse-grained molecular dynamics simulations indicate that dopant molecules are more likely to disperse in the polar environment of triethylene glycol chains than in the apolar environment of the alkyl chains. Thus, an improved atomic force microscopy (AFM) morphology with reduced phase separation was observed for the doped NDI-based copolymer with polar side chains. We argued that an intimate contact between the host and the dopant molecules in the NDI-based copolymer with polar side chains facilitates the molecular doping and gives rise to an improved electrical conductivity. Our work demonstrates the role that polar side chains play in successful n-doping of D–A copolymers and provides a guideline for side chains which may influence the charging behavior.

We synthesized a modified N2200 copolymer bearing polar triethylene glycol-based side chains (see synthetic details in the Supporting Information), which we called TEG-N2200. The chemical structure of TEG-N2200 is displayed together with those of N2200 with the traditional alkyl side chains and n-DMBI dopant in **Figure 1**a. Figure 1b shows the cyclic voltammetry characterization of N2200 and TEG-N2200 thin films. The first half-wave reduction potentials (potential in electron volts vs Fc/Fc^+) are −1.04 eV for N2200, which agrees with the literature,[32,42] and −1.11 eV for TEG-N2200. The estimated LUMO levels of N2200 and TEG-N2200 are −3.76 and −3.69 eV, respectively. The deep LUMO levels confirm the strong electron affinity of the NDI core. A slight upshift of the LUMO level is observed from N2200 to TEG-N2200, which is attributed to the stronger electron-donating character of the TEG side chains as compared to alkyl side chain to the polymer backbone.[43] It is believed that charges are actually transferred from the singly occupied molecular orbital level (−2.36 eV) of n-DMBI to the LUMO level of host molecules upon activation of the doping.[44] Therefore, both D–A copolymers are expected to be efficiently doped by n-DMBI from a view point of energetics. Figure 1c,d displays the UV–vis–NIR absorption coefficient spectra of pristine N2200 and TEG-N2200 thin films and those varyingly doped by n-DMBI, respectively. Pristine N2200 thin film showed two characteristic neutral peaks at 390 and 706 nm, which we assign to the π–π^* transition and charge transfer transition, respectively.[38] As N2200 thin films are doped with more n-DMBI, these neutral spectra peaks are gradually bleached, which is accompanied by the appearance of two absorption bands located at ≈500 and 820 nm. These new spectral features are attributed to the polaron-induced transitions, in accord with previous studies.[38] The pristine TEG-N2200 thin film exhibits similar absorption peaks (391 and 704 nm), but with enhanced intensities and reduced line widths with respect to the N2200 thin film, possibly caused by a modified π–π^* stacking or molecular alignment induced by the polar side chains.[45] Additionally, the absorption onset of the TEG-N2200 thin film becomes redshifted and less steep compared to that of the N2200 thin film. For the doped TEG-N2200 thin films, the high-energy signal of polaron-induced absorptionat ≈500 nm is also observed, while the low-energy signal is not visible. The reason for the latter is not clear at this stage. Additionally, n-doping of the TEG-N2200 thin films shows more pronounced bleaching of the neutral peaks at ≈390 and 705 nm than doping of the N2200 thin films, indicating increased doping levels.

The work functions of the N2200 and TEG-N2200 thin films doped from 0.36 to 71 mol % were measured using Kelvin probe on Au layers as shown in Figure S4 (Supporting Information). As the carrier densities in the pristine organic layers were very low, it is impossible to obtain accurate work functions in the pristine states. It is assumed that the Fermi level in the pristine material is roughly located in the middle of the bandgap. Considering their similar LUMO levels and bandgaps, a Fermi level of ≈−4.5 eV is speculated for the two pristine copolymers. Doped TEG-N2200 thin films exhibit lower work functions than the doped N2200 thin films at the same doping concentrations, which indicates increased doping levels for the former, which is consistent with absorption spectra analysis.

Figure 2a shows the electrical conductivities (σ) of the doped N2200 and TEG-N2200 thin films at different doping concentrations. At a doping concentration of 7.1 mol%, the doped TEG-N2200 layer exhibits an average σ of 1.5×10^{-4} S cm^{-1}, which is much higher than that (1.6×10^{-6} S cm^{-1}) of the doped N2200 layer. As the doping concentration increases, the electrical conductivities of both the doped thin films gradually increase. The doped N2200 layer achieves a highest average σ of 8.6×10^{-4} S cm^{-1} at a doping concentration of 56 mol%, which is consistent with previously reported values.[34,35] An optimized averaged σ of 0.17 S cm^{-1} is obtained from the 71%-doped TEG-N2200 thin film, which represents a 200-fold increase with respect to the doped N2200 thin film and the highest electrical conductivity for the class of n-doped D–A copolymers. The charge transport in the doped films is thermally activated with activation energies of 261 and 160 meV for the 71%-doped N2200 and TEG-N2200, respectively. The smaller activation energy observed for

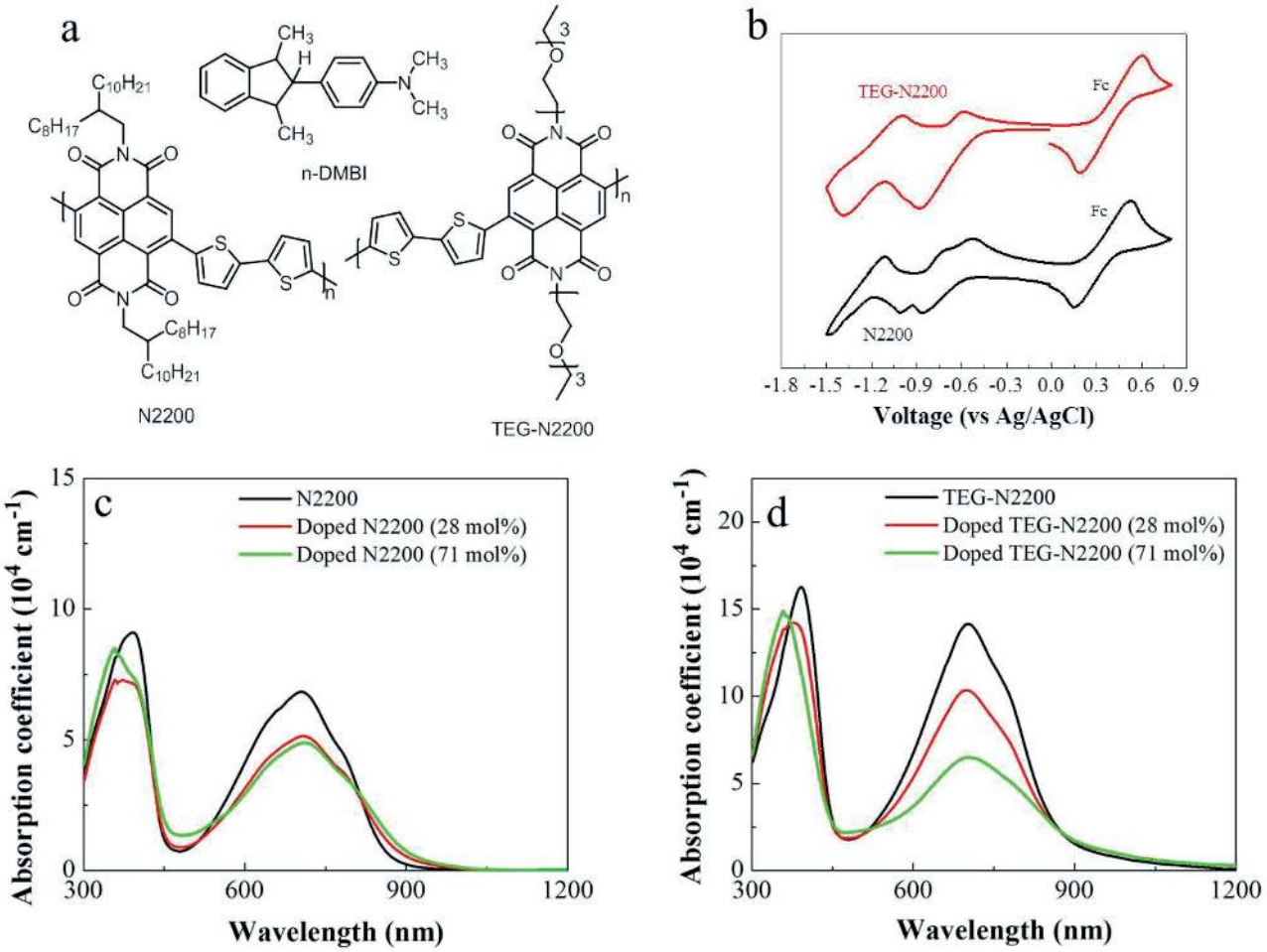

Figure 1. a) The chemical structures of N2200, n-DMBI, and TEG-N2200; b) cyclic voltammograms; the UV–vis–NIR absorption coefficient spectra of pristine and doped N2200 c) and TEG-N2200 d) thin films.

the doped TEG-N2200 indicates that more charge carriers are generated by the molecular doping.[46] Additionally, we carried out field-effect mobility measurements for pristine N2200 and TEG-N2200 thin films using a bottom contact/top gate geometry, as displayed in Figure S5 (Supporting Information). The pristine N2200 layer exhibited a μ of 7.2×10^{-3} $cm^2(Vs)^{-1}$ in the saturated regime, which is a typical value for the chloroform-processed N2200 layer.[47] Although the TEG-N2200-based transistor shows more "textbook" characteristics than the N2200-based devices do, the former exhibits an inferior μ of 2.2×10^{-4} $cm^2(Vs)^{-1}$. Therefore, we argue that the differences in the conductivity of two doped D–A copolymers are not caused by their intrinsic charge transport properties, but related to the extrinsic molecular doping.

The Seebeck coefficient (S) is determined by the difference between the Fermi level energy (E_F) and the charge transport energy (E_T).[48] As the doping level increases from molecular doping, more charges are generated, which shifts E_F toward E_T and decreases the absolute S value. Therefore, the Seebeck coefficient is usually considered an important parameter for evaluating the doping level. We measured S values for varyingly doped N2200 and TEG-N2200 thin films, which are displayed in Figure 2b (see details in Figure S6 in the Supporting Information). Notably, we used a steady-state method to obtain the thermal voltages, which excluded any transient ionic Seebeck effects and improved the accuracy of the measurements.[49] The Seebeck coefficient of the doped N2200 layers can be changed from -894 ± 6 to -292 ± 4 $\mu V\ K^{-1}$ by modulating the doping concentration from 14 to 71 mol%. For doped TEG-N2200 thin films, S varied from -433 ± 3 $\mu V\ K^{-1}$ at a doping concentration of 7.1 mol% to -111 ± 0.6 $\mu V\ K^{-1}$ at a doping concentration of 85 mol%. Both doped D–A copolymer films display negative S values, indicating n-type doping with electrons as the charge carrier. Doped TEG-N2200 layers exhibit much lower absolute S than those of doped N2200 layers, which clearly indicates higher doping levels and it agrees well with previous results. Note that the doped N2200 layer shows an optimized power factor of only 0.01 $\mu W\ m^{-1}\ K^{-2}$ at a doping concentration of 56 mol%, which is consistent with the previous study;[38] while doping TEG-N2200 gives a maximum power factor of 0.40 $\mu W\ m^{-1}\ K^{-2}$ at 56 mol%. Although the power factor of the doped TEG-N2200 layer still lags behind those of doped copolymers without any D–A character due due to its low carrier mobility, we open a new pathway to engineer the doping level of D–A copolymers to advance their applications in thermoelectric and optoelectronic devices.

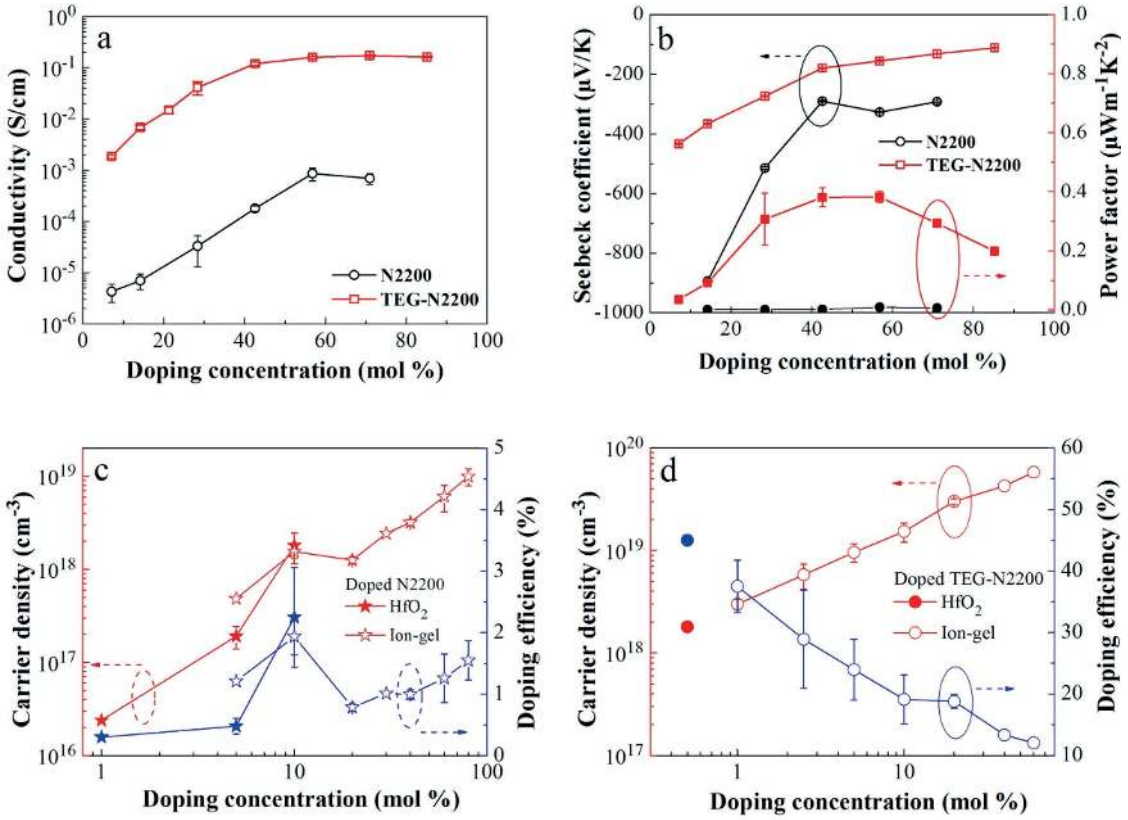

Figure 2. The electrical conductivities a) and Seebeck coefficient and power factor b) of differently doped N2200 and TEG-N2200 layers; c) and d) carrier densities extracted from MIS devices based on HfO_2 (filled symbols) and ion–gel dielectric layers (open symbols) and corresponding doping efficiencies as a function of doping concentration in differently doped N2200 films and doped TEG-N2200 films. The total density of 8×10^{20} cm^{-3} is used for both D–A copolymers.

To directly measure carrier densities of various doped films, we employ admittance spectroscopy to metal–insulator–semiconductor (MIS) structured devices. The scope of carrier density extracted by this method is mainly determined by the capacitance of the used insulator according to the Mott–Schottky equation (see the Experimental Section). We used high-k HfO_2 and for the first time an ion–gel layer, which has a one order of magnitude higher capacitance than the former, as the insulator of MIS devices (see Figure S7 in the Supporting Information). The carrier densities and corresponding doping efficiencies for differently doped N2200 and TEG-N2200 layers are displayed in Figure 2c,d, respectively. Doped N2200 films at the doping concentration ranging from 10 to 60 mol% show carrier densities falling between 10^{18} cm^{-3} and 10^{19} cm^{-3} while doped TEG-N2200 films have carrier densities (>10^{19} cm^{-3}) of ≈10 times higher than those of doped N2200 films at same doping concentrations. To our knowledge, this is the first time to directly measure the carrier density in molecularly doped organic films at high doping concentrations. Doped TEG-N2200 layers show doping efficiencies of >10%, which are more than one order of magnitude higher than those (≈1%) of doped N2200. These results highlight not only the effectiveness of ion gel-based MIS devices for directly extracting carrier density in heavily doped films, but also benefits of the polar side chains for improving n-doping of D–A copolymers.

We analyzed the surface morphologies of the pristine and differently doped N2200 and TEG-N2200 thin films by AFM as displayed in **Figure 3** and Figures S8 and S9 in the Supporting Information. The pristine N2200 film shows a fibril-textured morphology, implying long-range order,[50] while small nodules are observed in pristine TEG-N2200 film. The difference in morphology may explain the origin of the higher carrier mobility of pristine N2200 with respect to TEG-N2200. The doped N2200 films show lower threshold doping concentration (≈14%) for observing surface aggregates than the doped TEG-N2200 (≈42%). These aggregations are considered to be caused by the phase separation between the undoped host matrix and polar dopant/doping products, which is driven by surface energy differences.[23,51] As shown in Figure 3c, many small spherical aggregates are ubiquitously dispersed on 42 mol%-doped N2200 film (marked by white rectangle). These spherical aggregates are presumably caused by the poor solubility of the polar dopant in the N2200 matrix.[34] In contrast, 42 mol%-doped TEG-N2200 film shows a very clean surface morphology except for few large aggregates. Recently, ethylene glycol-based side chains have been reported to increase the polarities of conjugated polymers in electrochemical transistor devices and organic p-type doped systems.[28,52] We argued that polar n-DMBI molecules can be more easily dispersed in the TEG-N2200 matrix because of the hydrophilic triethylene glycol-based side chains than in N2200, with its hydrophobic

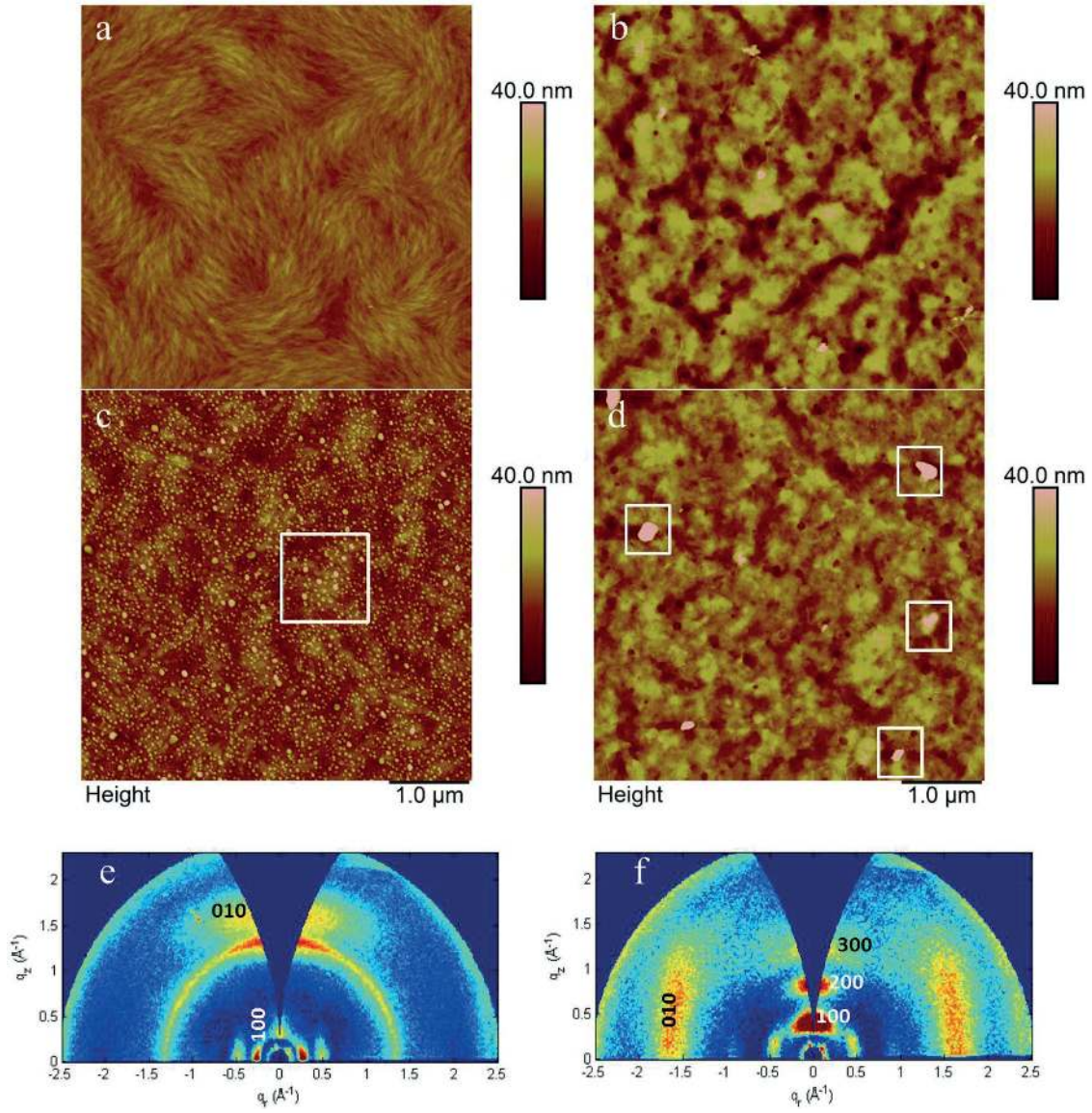

Figure 3. Topographic AFM morphology images of pristine N2200 a) and TEG-N2200 b) films, and doped N2200 c) and doped TEG-N2200 d) at a doping concentration of 42 mol%; 2D GIWAXS patterns for the pristine N2200 e) and TEG-N2200 f) thin films. The numbers are indicative of the hkl miller indices for the crystallographic planes.

alkyl side chains. Since the two D–A copolymers exhibit similar LUMO levels, the doping process is mainly influenced by the quality of mixing between the host and dopant molecules. The improved mixing of the TEG-N2200/n-DMBI blend facilitates doping with an improved doping efficiency and thus causes an enhanced conductivity as compared to the N2200/n-DMBI blend.

The influences of side chains and doping process on molecular packing of the two D–A copolymers were studied by grazing incidence wide angle x-ray scattering (GIWAXS). The GIWAXS patterns and relative intensity cuts are shown in Figure 3e,f and Figure S10 in the Supporting Information. Clearly, N2200 mainly packs in a face-on orientation, in agreement with what is reported in the literature,[53] as evidenced by the orientation of the (100) reflection along the horizonthal q_y direction. On the contrary, TEG-N2200 stacks edge-on relative to substrate, (100) reflection along the vertical q_z direction. Both pristine D–A copolymers show clear (010) reflection, associated with a π–π stacking distance between molecules of about 3.9 Å. The difference in side-chain length between the two polymers is responsible for the different (100) lamellar spacing of 24 and 16 Å for N2200 and TEG-N2200, respectively. The doping process does not appear to significantly change the molecular orientations of the two polymers, having an influence only on the extent of developed crystallinity. For TEG-N2200, the (010) spacing remains unchanged upon doping and (100) spacing along q_z direction is only slightly increased to 17 Å. This finding indicates that polar n-DMBI dopants are mainly incorporated in polar side chains because of their similar polarities, which is favorable for in-plane charge transport. Additionally, the

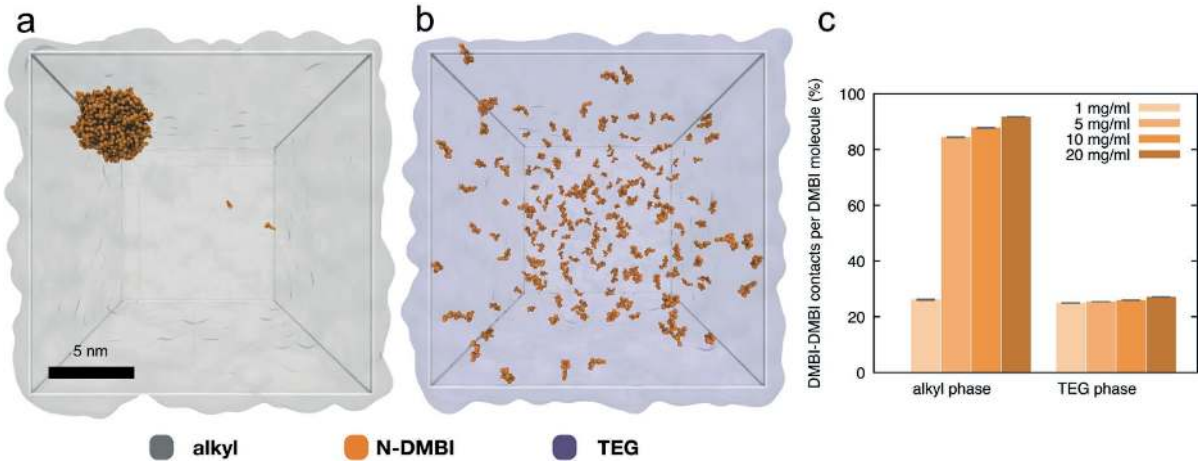

Figure 4. Representative snapshots of coarse-grained molecular dynamics simulations of n-DMBI molecules dissolved in a) a pure N2200 side chain phase and b) a pure TEG-N2200 side chain phase. The normalized number of contacts between dopant molecules in the two phases at different concentrations is also shown c).

crystallization of N2200 is more disturbed by doping than that of TEG-N2200 as observed from the linecuts in Figure S10 (Supporting Information).

To investigate the effect that the microenvironments created by the two different side chains may exert on the dopant molecules, we performed coarse-grained molecular dynamics simulations. To this end, we set up systems where different concentrations of n-DMBI molecules are solvated in a pure phase of side chains of either N2200 or TEG-N2200. The models employed are based on the Martini force field,[54] a transferable coarse-grained force field parametrized based on thermodynamic data that is widely used to study carbon nanostructures, polymers, and soft heterojunction materials.[55–58] More details on the force field and coarse-grained models are given in the Supporting Information. Representative snapshots of simulations which have reached equilibrium are shown in **Figure 4**a (alkyl) and b (TEG). The molecular dynamics simulations showed a rather high tendency for the dopant molecules to cluster in the alkyl phase, where molecules quickly form small cluster which, if given enough time, then further cluster together. By contrast, the TEG phase is a much better solvent for n-DMBI, with molecules being well dispersed up to concentrations of 20 mg mL^{-1}, as quantified by the number of contacts between dopant molecules shown in Figure 4c. From n-DMBI solvation-free energies (calculated via thermodynamic integration as described in the Supporting Information) in either of the two phases, the free energy of transfer required to move an n-DMBI molecule from the alkyl to the TEG phase was found to be −16 kJ mol^{-1}, quantifying further the strong preference for the TEG phase over the alkyl one, which was already evident from the equilibrium simulation results. Furthermore, to exclude any effect of the length or branching of the side chains on the dispersion of n-DMBI molecules, we performed additional simulations with phases of ethylene glycol and alkyl side chains of different length and branching degree. The results, shown in Figure S11 in the Supporting Informatin, confirm the findings of Figure 4, consolidating the fact that the effect depends solely on the polarity of the side chain. The higher TEG-solubility seems to be the consequence of the molecular structure of n-DMBI, containing imidazole and amine groups, make this dopant moderately polar. Molecular dynamics simulations thus indicate a rather strong tendency for the apolar alkyl environment to induce clustering of the dopant molecules, as opposed to the polar TEG phase which instead favors the molecular dispersion of n-DMBI. In view of these results, the small aggregates noted in the AFM images of doped N2200 films could be ascribed to n-DMBI molecules.

To achieve a deeper understanding of the charge transport in this system, we measured the variable-temperature electrical conductivity and Seebeck coefficient of the doped TEG-N2200 layer. The electrical conductivity due to hopping in disordered materials is temperature dependent[3,59]

$$\sigma = \sigma_0 \exp\left(-\left(\frac{T_0}{T}\right)^s\right) \quad (1)$$

Here, σ_0 and T_0 are the preexponential factor and the characteristic temperature, respectively. s is a hopping exponent related to different charge transport behaviors: (1) $s = 0.25$ represents 3D Mott variable-range hopping (VRH) transport; (2) $s = 1$ for nearest-neighbor hopping (NNH) featuring thermally activated transport. The temperature-dependent conductivity of the 71%-doped TEG-N2200 layer can be well described by the 3D Mott VRH model with $s = 0.25$, as shown in **Figure 5**a. The inset of Figure 5a shows a similar s of 0.24 based on an approach by Zabrodskii and Zinoveva.[59] For a 3D Mott VRH system, the absolute Seebeck coefficient linearly increases with $T^{0.5}$.[60,61] However, we observed that the absolute Seebeck coefficient linearly increases with $1/T$ in the 71%-doped TEG-N2200 layer, as shown in Figure 5b (see details in Figure S13, Supporting Information), largely violating the 3D Mott VRH theory. A weak dependence of S on temperature ($\partial S/(1/T) = 35$ meV) in the doped TEG-N2200 layer and well-defined lamellar crystals from GIWAXS study indicate low molecular disorder,[38] which makes NNH more likely for charge transport. In Figure 5c, the doped TEG-N2200 follows the empirical relation of $S \propto \sigma^{-1/4}$, which has already been observed for other semiconducting polymers,[7,28,38] while Mott VRH gave a different $S - \sigma$ relationship

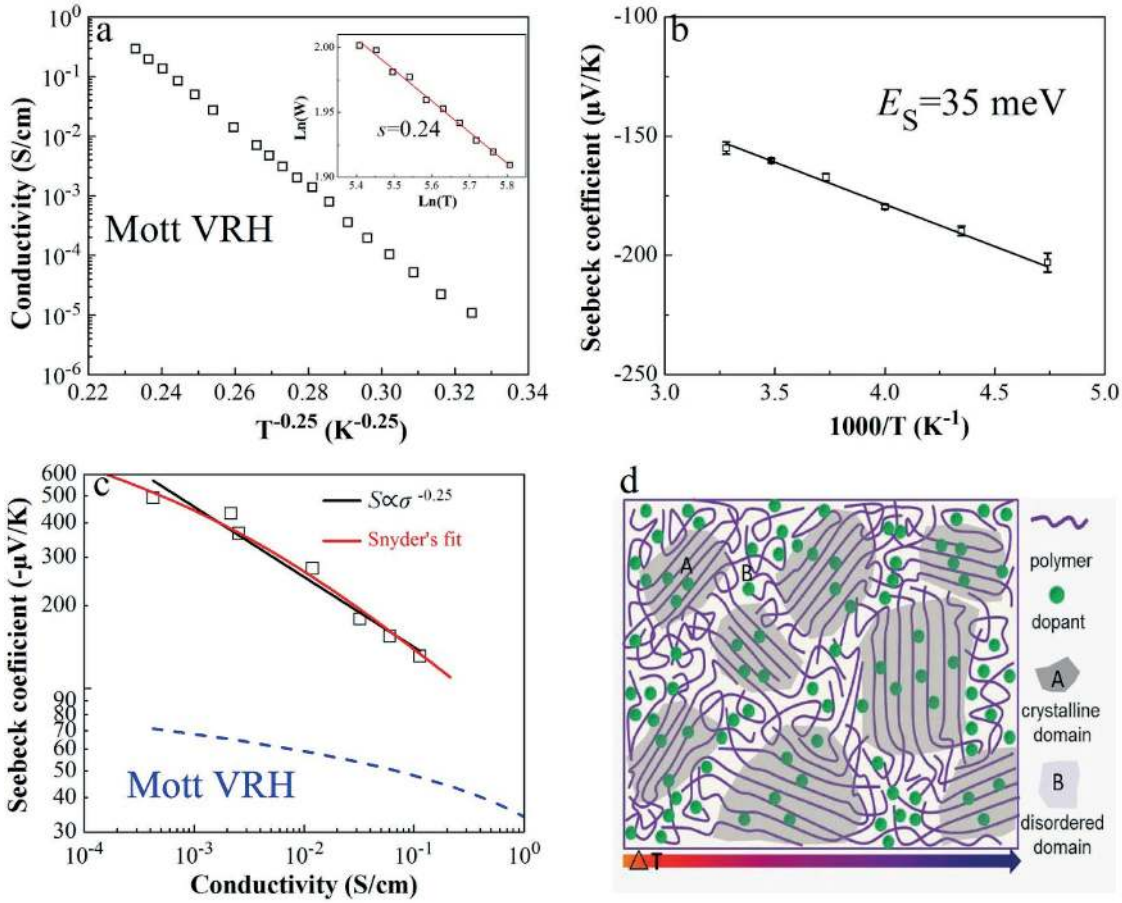

Figure 5. The temperature dependence of the electrical conductivity a) and Seebeck coefficient b) of the 71 mol%-doped TEG-N2200 thin film; c) a plot of the Seebeck coefficient versus the electrical conductivity of doped TEG-N2200 from the simulation based on 3D Mott VRH (blue dashed line) and experiment (open symbol), and fittings of experimental data by the empirical relation ($S \propto \sigma^{-0.25}$) and Snyder's model (transport parameter = 3 and $\sigma_{E0} = 5 \times 10^{-4}$ S cm^{-1}); and d) a schematic presentation of the heterogeneous thermoelectric transport regions.

(blue dashed line, obtained using a method similar to one previously reported).[7,62] The empirical trend also implies low molecular disorder.[7,38,63]

The characteristic temperature-dependence analysis of the electrical conductivity and Seebeck coefficient in the doped TEG-N2200 system revealed seemingly contradicting charge transport mechanisms, which may suggest a heterogeneous thermoelectric transport.[61] As proposed in Figure 5d, the doped TEG-N2200 film might have NNH dominated transport regions with relatively high molecular order interspersed by disordered domains featuring 3D Mott VRH transport, which agrees with AFM morphology (Figure 3b), GIWAXS data, and the microstructural pictures of the typical semicrystalline polymers.[62,64] It is noted that, due to the absence of tie molecules between adjacent ordered domains, the charge transport across the disordered domains dominates carrier conduction as the rate-limiting step, which is evidenced by the low electron mobility. Therefore, we observed 3D Mott VRH-dominated charge transport from the variable-temperature conductivity experiments. However, the Seebeck coefficient mainly originates from the ordered regions and shows NNH transport behavior because the Mott VRH regions only makes up a small portion of the total contribution (see the blue dashed line in Figure 5c). Additionally, the $S - \sigma$ relationship in Figure 5c can be well fitted by Snyder's model using a transport parameter value of 3 and transport coefficient of $\sigma_{E0} = 5 \times 10^{-4}$ S cm^{-1}.[62] The small σ_{E0} value indicates a poor percolation of charge carriers from ordered regions through disordered regions, which further validates the heterogeneous model. This heterogeneous model can well explain the thermoelectric transport observed in doped TEG-N2200 and suggests a possible direction for simultaneously improving S and σ by tuning the morphology of doped TEG-N2200, which is beyond the scope of this work.

In summary, for the first time we demonstrated that the molecular n-doping of an NDI-based copolymer can be greatly improved to produce a 200-fold enhancement in the electrical conductivity by rationally tailoring the side chains without changing the D–A backbone. We replaced the traditional alkyl side chains of N2200 with the polar triethylene glycol-based side chains and achieved a high electrical conductivity of 0.17 S cm^{-1} upon n-DMBI doping, which is the highest reported for n-type D–A copolymers. UV–vis absorption spectra, work function, direct measurements of carrier densities, and Seebeck coefficient measurements confirmed the increased doping level as the primary cause for the improved electrical conductivity. The coarse-grained molecular dynamics simulations indicated

that the polar side chains could greatly reduce the clustering of n-DMBI molecules and favor the dispersion of the dopant into the host matrix. Accordingly, intimate contact between the host and dopant molecules in the NDI-based copolymer system with the polar side chains facilitates the molecular doping and improves the electrical conductivity. The charge transport mechanism of the doped TEG-N2200 film was analyzed with a proposed morphologically heterogeneous model, which suggests a method for further promoting thermoelectric properties of n-doped D–A copolymers. Our work emphasizes role of the polar side chains of D–A copolymers in n-doping and provides a guideline for designing efficient n-type D–A copolymers for advancing organic electronics.

Experimental Section

Materials: TEG-N2200 was synthesized in our lab. ActivInk N2200 and n-DMBI were purchased from Flexterra, Inc. and Sigma-Aldrich, respectively.

Computational Methods: Classical coarse-grained molecular dynamics simulations were carried out using a new major version of the Martini[54] force field soon to be published. The n-DMBI model was based on the model developed in our recent work.[65] Bonded parameters for the TEG model were taken from the literature.[66,67] All the details for the coarse-grained particle types employed in this study are reported in the Supporting Information, as well as all the files needed to reproduce the simulation results. Simulations were performed using the GROMACS 2016.x software package,[68] keeping constant pressure and temperature at 1 bar and 298 K, respectively. A time step of 20 fs was used to integrate the equations of motion. All simulation parameters correspond to the "new" Martini set of run parameters.[69] The number of contacts has been computed from 400 ns of equilibrated simulations (which were at least 1.2 µs long in total). n-DMBI–n-DMBI contacts per n-DMBI molecule were normalized with respect to their number in a pure n-DMBI phase.

Conductivity and Carrier Density Measurement: For the electrical conductivity measurements, parallel line-shape Au electrodes with a width (w) of 13 mm and a channel length (L) of 100–300 µm were deposited as the bottom contact before spin coating. Voltage-sourced two-point conductivity measurements were conducted with a probe station in a N_2 glovebox, and the variable-temperature conductivity was measured under vacuum in a cryogenic probe station. The electrical conductivity (σ) was calculated according to the formula: $\sigma = (J/V) \times L/(w \times d)$. The conductivity reported in this work was averaged from six devices. The charge carrier densities (n) in doped films were measured from admittance spectroscopy of metal–insulator–semiconductor architecture (ITO/insulator/doped active layer/Al) combined with Mott–Schottky analysis[70]

$$n = \frac{2}{e\varepsilon_0\varepsilon_r \frac{\partial C_p^{-2}}{\partial V}} \tag{2}$$

where ε_r and C_p are dieledtric constant of active layer and capacitance of MIS devices. The capacitance–voltage (C_p–V) measurements were conducted at a frequency of 200 and 10 Hz for HfO_2 and ion gel-based MIS devices, respectively (see the details of preparing HfO_2 and ion gel insulator in the Supporting Information).

Supporting Information

Supporting Information is available from the Wiley Online Library or from the author.

Acknowledgements

J.L. and L.Q. contributed equally to this work. This is a publication by the FOM Focus Group "Next Generation Organic Photovoltaics", participating in the Dutch Institute for Fundamental Energy Research (DIFFER). R.A. thank NWO (Graduate Programme Advanced Materials, No. 022.005.006) for financial support. Computational resources for this work were partly provided by the Dutch National Supercomputing Facilities through NWO.

Conflict of Interest

The authors declare no conflict of interest.

Keywords

donor–acceptor copolymer, electrical conductivity and doping level, n-type doping, solution processing

Received: August 15, 2017
Revised: November 2, 2017
Published online: January 11, 2018

[1] I. Salzmann, G. Heimel, M. Oehzelt, S. Winkler, N. Koch, *Acc. Chem. Res.* **2016**, *49*, 370.
[2] P. Pingel, D. Neher, *Phys. Rev. B* **2013**, *87*, 115209.
[3] K. Kang, S. Watanabe, K. Broch, A. Sepe, A. Brown, I. Nasrallah, M. Nikolka, Z. Fei, M. Heeney, D. Matsumoto, K. Marumoto, H. Tanaka, S.-I. Kuroda, H. Sirringhaus, *Nat. Mater.* **2016**, *15*, 896.
[4] M. L. Tietze, P. Pahner, K. Schmidt, K. Leo, B. Lüssem, *Adv. Funct. Mater.* **2015**, *25*, 2701.
[5] Y. Xuan, X. Liu, S. Desbief, P. Leclère, M. Fahlman, R. Lazzaroni, M. Berggren, J. Cornil, D. Emin, X. Crispin, *Phys. Rev. B* **2010**, *82*, 115454.
[6] S. Fabiano, S. Braun, X. Liu, E. Weverberghs, P. Gerbaux, M. Fahlman, M. Berggren, X. Crispin, *Adv. Mater.* **2014**, *26*, 6000.
[7] A. M. Glaudell, J. E. Cochran, S. N. Patel, M. L. Chabinyc, *Adv. Energy Mater.* **2015**, *5*.
[8] B. Lüssem, M. Riede, K. Leo, *Phys. Status Solidi* **2013**, *210*, 9.
[9] M. Culebras, C. Gómez, A. Cantarero, *Materials* **2014**, *7*, 6701.
[10] J. Yang, H.-L. Yip, A. K.-Y. Jen, *Adv. Energy Mater.* **2013**, *3*, 549.
[11] B. Lüssem, M. L. Tietze, H. Kleemann, C. Hoßbach, J. W. Bartha, A. Zakhidov, K. Leo, *Nat. Commun.* **2013**, *4*, 2775.
[12] G.-H. Kim, L. Shao, K. Zhang, K. P. Pipe, *Nat. Mater.* **2013**, *12*, 719.
[13] A. A. Günther, M. Sawatzki, P. Formánek, D. Kasemann, K. Leo, *Adv. Funct. Mater.* **2016**, *26*, 768.
[14] B. A. Jones, M. J. Ahrens, M.-H. Yoon, A. Facchetti, T. J. Marks, M. R. Wasielewski, *Angew. Chem.* **2004**, *116*, 6523.
[15] G. Lu, J. Blakesley, S. Himmelberger, P. Pingel, J. Frisch, I. Lieberwirth, I. Salzmann, M. Oehzelt, R. Di Pietro, A. Salleo, N. Koch, D. Neher, *Nat. Commun.* **2013**, *4*, 1588.
[16] T. Takenobu, T. Takano, M. Shiraishi, Y. Murakami, M. Ata, H. Kataura, Y. Achiba, Y. Iwasa, *Nat. Mater.* **2003**, *2*, 683.
[17] M. Nikolka, I. Nasrallah, B. Rose, M. K. Ravva, K. Broch, A. Sadhanala, D. Harkin, J. Charmet, M. Hurhangee, A. Brown, S. Illig, P. Too, J. Jongman, I. McCulloch, J.-L. Bredas, H. Sirringhaus, *Nat. Mater.* **2016**, *16*, 356.
[18] S. N. Patel, A. M. Glaudell, K. A. Peterson, E. M. Thomas, K. A. O'Hara, E. Lim, M. L. Chabinyc, *Sci. Adv.* **2017**, *3*, e1700434.
[19] Y. Pei, X. Shi, A. LaLonde, H. Wang, L. Chen, G. J. Snyder, *Nature* **2011**, *473*, 66.

[20] D. Huang, H. Yao, Y. Cui, Y. Zou, F. Zhang, C. Wang, H. Shen, W. Jin, J. Zhu, Y. Diao, W. Xu, C. Di, D. Zhu, *J. Am. Chem. Soc.* **2017**, *139*, 13013.
[21] D. Di Nuzzo, C. Fontanesi, R. Jones, S. Allard, I. Dumsch, U. Scherf, E. von Hauff, S. Schumacher, E. Da Como, *Nat. Commun.* **2015**, *6*, 6460.
[22] K. Shi, F. Zhang, C.-A. Di, T.-W. Yan, Y. Zou, X. Zhou, D. Zhu, J.-Y. Wang, J. Pei, *J. Am. Chem. Soc.* **2015**, *137*, 6979.
[23] B. D. Naab, S. Guo, S. Olthof, E. G. B. Evans, P. Wei, G. L. Millhauser, A. Kahn, S. Barlow, S. R. Marder, Z. Bao, *J. Am. Chem. Soc.* **2013**, *135*, 15018.
[24] D. T. Duong, H. Phan, D. Hanifi, P. S. Jo, T.-Q. Nguyen, A. Salleo, *Adv. Mater.* **2014**, *26*, 6069.
[25] Y. Karpov, T. Erdmann, I. Raguzin, M. Al-Hussein, M. Binner, U. Lappan, M. Stamm, K. L. Gerasimov, T. Beryozkina, V. Bakulev, D. V. Anokhin, D. A. Ivanov, F. Günther, S. Gemming, G. Seifert, B. Voit, R. Di Pietro, A. Kiriy, *Adv. Mater.* **2016**, *28*, 6003.
[26] I. E. Jacobs, E. W. Aasen, J. L. Oliveira, T. N. Fonseca, J. D. Roehling, J. Li, G. Zhang, M. P. Augustine, M. Mascal, A. J. Moule, *J. Mater. Chem. C* **2016**, *4*, 3454.
[27] L. Müller, D. Nanova, T. Glaser, S. Beck, A. Pucci, A. K. Kast, R. R. Schröder, E. Mankel, P. Pingel, D. Neher, W. Kowalsky, R. Lovrincic, *Chem. Mater.* **2016**, *28*, 4432.
[28] R. Kroon, D. Kiefer, D. Stegerer, L. Yu, M. Sommer, C. Müller, *Adv. Mater.* **2017**, *29*, 1700930.
[29] Y. Deng, Y. Chen, X. Zhang, H. Tian, C. Bao, D. Yan, Y. Geng, F. Wang, *Macromolecules* **2012**, *45*, 8621.
[30] Y. Deng, J. Liu, J. Wang, L. Liu, W. Li, H. Tian, X. Zhang, Z. Xie, Y. Geng, F. Wang, *Adv. Mater.* **2014**, *26*, 471.
[31] Y. Li, *Acc. Chem. Res.* **2012**, *45*, 723.
[32] H. Yan, Z. Chen, Y. Zheng, C. Newman, J. R. Quinn, F. Dötz, M. Kastler, A. Facchetti, *Nature* **2009**, *457*, 679.
[33] H. N. Tsao, D. M. Cho, I. Park, M. R. Hansen, A. Mavrinskiy, D. Y. Yoon, R. Graf, W. Pisula, H. W. Spiess, K. Müllen, *J. Am. Chem. Soc.* **2011**, *133*, 2605.
[34] R. a. Schlitz, F. G. Brunetti, A. M. Glaudell, P. L. Miller, M. a. Brady, C. J. Takacs, C. J. Hawker, M. L. Chabinyc, *Adv. Mater.* **2014**, *26*, 2825.
[35] B. D. Naab, X. Gu, T. Kurosawa, J. W. F. To, A. Salleo, Z. Bao, *Adv. Electron. Mater.* **2016**, *2*, 1600004.
[36] B. D. Naab, S. Zhang, K. Vandewal, A. Salleo, S. Barlow, S. R. Marder, Z. Bao, *Adv. Mater.* **2014**, *26*, 4268.
[37] Y. Wang, M. Nakano, T. Michinobu, Y. Kiyota, T. Mori, K. Takimiya, *Macromolecules* **2017**, *50*, 857.
[38] S. Wang, H. Sun, U. Ail, M. Vagin, P. O. Å. Persson, J. W. Andreasen, W. Thiel, M. Berggren, X. Crispin, D. Fazzi, S. Fabiano, *Adv. Mater.* **2016**, *28*, 10764.
[39] R. Steyrleuthner, M. Schubert, I. Howard, B. Klaumünzer, K. Schilling, Z. Chen, P. Saalfrank, F. Laquai, A. Facchetti, D. Neher, *J. Am. Chem. Soc.* **2012**, *134*, 18303.
[40] L. A. Estrada, D. Y. Liu, D. H. Salazar, A. L. Dyer, J. R. Reynolds, *Macromolecules* **2012**, *45*, 8211.
[41] C. J. DuBois, J. R. Reynolds, *Adv. Mater.* **2002**, *14*, 1844.
[42] X. Guo, M. D. Watson, *Org. Lett.* **2008**, *10*, 5333.
[43] W.-H. Chang, J. Gao, L. Dou, C.-C. Chen, Y. Liu, Y. Yang, *Adv. Energy Mater.* **2014**, *4*, 1300864.
[44] P. Wei, J. H. Oh, G. Dong, Z. Bao, *J. Am. Chem. Soc.* **2010**, *132*, 8852.
[45] B. Meng, H. Song, X. Chen, Z. Xie, J. Liu, L. Wang, *Macromolecules* **2015**, *48*, 4357.
[46] W. F. Pasveer, J. Cottaar, C. Tanase, R. Coehoorn, P. A. Bobbert, P. W. M. Blom, D. M. de Leeuw, M. A. J. Michels, *Phys. Rev. Lett.* **2005**, *94*, 206601.
[47] S. Fabiano, H. Yoshida, Z. Chen, A. Facchetti, M. A. Loi, *ACS Appl. Mater. Interfaces* **2013**, *5*, 4417.
[48] G. Kim, K. P. Pipe, *Phys. Rev. B* **2012**, *86*, 85208.
[49] H. Wang, U. Ail, R. Gabrielsson, M. Berggren, X. Crispin, *Adv. Energy Mater.* **2015**, *5*, 1500044.
[50] A. Luzio, L. Criante, V. D'Innocenzo, M. Caironi, R. H. Friend, *Sci. Rep.* **2013**, *3*, 125204.
[51] J. Liu, L. Qiu, G. Portale, M. Koopmans, G. ten Brink, J. C. Hummelen, L. J. A. Koster, *Adv. Mater.* **2017**, *29*, 1701641.
[52] A. Giovannitti, C. B. Nielsen, D.-T. Sbircea, S. Inal, M. Donahue, M. R. Niazi, D. A. Hanifi, A. Amassian, G. G. Malliaras, J. Rivnay, I. McCulloch, *Nat. Commun.* **2016**, *7*, 13066.
[53] J. Rivnay, M. F. Toney, Y. Zheng, I. V. Kauvar, Z. Chen, V. Wagner, A. Facchetti, A. Salleo, *Adv. Mater.* **2010**, *22*, 4359.
[54] S. J. Marrink, H. J. Risselada, S. Yefimov, D. P. Tieleman, A. H. De Vries, *J. Phys. Chem. B* **2007**, *111*, 7812.
[55] M. Lelimousin, M. S. P. Sansom, *Small* **2013**, *9*, 3639.
[56] D. Bochicchio, G. M. Pavan, *ACS Nano* **2017**, *11*, 1000.
[57] T. Winands, M. Böckmann, T. Schemme, P.-M. T. Ly, D. H. de Jong, Z. Wang, C. Denz, A. Heuer, N. L. Doltsinis, *Phys. Chem. Chem. Phys.* **2016**, *18*, 6217.
[58] R. Alessandri, J. J. Uusitalo, A. H. De Vries, R. W. A. Havenith, S. J. Marrink, *J. Am. Chem. Soc.* **2017**, *139*, 3697.
[59] A. Yildiz, N. Serin, T. Serin, M. Kasap, *Jpn. J. Appl. Phys.* **2009**, *48*, 111203.
[60] A. J. Epstein, H. Rommelmann, R. Bigelow, H. W. Gibson, D. M. Hoffmann, D. B. Tanner, *Phys. Rev. Lett.* **1983**, *50*, 1866.
[61] A. B. Kaiser, *Phys. Rev. B* **1989**, *40*, 2806.
[62] S. Dongmin Kang, G. Jeffrey Snyder, *Nat. Mater.* **2017**, *16*, 252.
[63] N. Mateeva, H. Niculescu, J. Schlenoff, L. R. Testardi, *J. Appl. Phys.* **1998**, *83*, 3111.
[64] R. Noriega, J. Rivnay, K. Vandewal, F. P. V. Koch, N. Stingelin, P. Smith, M. F. Toney, A. Salleo, *Nat. Mater.* **2013**, *12*, 1038.
[65] L. Qiu, J. Liu, R. Alessandri, X. Qiu, M. Koopmans, R. W. A. Havenith, S. J. Marrink, R. C. Chiechi, L. J. Anton Koster, J. C. Hummelen, *J. Mater. Chem. A* **2017**, *5*, 21234.
[66] G. Rossi, P. F. J. Fuchs, J. Barnoud, L. Monticelli, *J. Phys. Chem. B* **2012**, *116*, 14353.
[67] M. Bulacu, N. Goga, W. Zhao, G. Rossi, L. Monticelli, X. Periole, D. P. Tieleman, S. J. Marrink, *J. Chem. Theory Comput.* **2013**, *9*, 3282.
[68] M. J. Abraham, T. Murtola, R. Schulz, S. Páll, J. C. Smith, B. Hess, E. Lindahl, *SoftwareX* **2015**, *1*, 19.
[69] D. H. de Jong, S. Baoukina, H. I. Ingólfsson, S. J. Marrink, *Comput. Phys. Commun.* **2016**, *199*, 1.
[70] P. Pingel, R. Schwarzl, D. Neher, *Appl. Phys. Lett.* **2012**, *100*, 143303.